

(compare Figs. 2A and 3). Nevertheless, in both environments there was no relation between ability to diversify and time spent evolving in the original high-nutrient media (Fig. 3) (sign tests of correlations between number of genotypes and transfer number for the six lines: $P > 0.2$ in both cases).

Adaptation can limit the ability of bacterial genotypes to diversify genetically. This was not the result of generalist evolution or the evolution of an intrinsic reduction in evolvability, but was caused by environment-specific adaptation. Given the strong empirical support for both the importance of environmental heterogeneity in diversification (7–14) and epistasis (6, 24), it is likely that rugged fitness landscapes, a requirement for the observed effects, are common. These results are therefore likely to be generally relevant and may help to explain patterns of diversity over both micro- and macroevolutionary time scales. Consistent with recent interpretations of macroevolutionary adaptive radiations (25), we predict that in environments that can potentially support similar levels of diversity, diversification is more likely to occur immediately following colonization of the environment than through expansion into new niches within the environment after an extinction event.

References and Notes

- H. Levene, *Am. Nat.* **87**, 331 (1953).
- P. W. Hedrick, M. E. Ginevan, E. P. Ewing, *Annu. Rev. Ecol. Syst.* **7**, 1 (1976).
- P. W. Hedrick, *Annu. Rev. Ecol. Syst.* **17**, 535 (1986).
- T. Dobzhansky, *Genetics and the Origin of Species* (Columbia Univ. Press, New York, 1937).
- M. C. Whitlock, P. C. Phillips, F. B. G. Moore, S. J. Tonsor, *Annu. Rev. Ecol. Syst.* **26**, 601 (1995).
- M. J. Wade, in *Epistasis and the Evolutionary Process*, J. B. Wolf, E. D. Brodie, M. J. Wade, Eds. (Oxford Univ. Press, Oxford, 2000), pp. 213–231.
- R. Korona, C. H. Nakatsu, L. J. Forney, R. E. Lenski, *Proc. Natl. Acad. Sci. U.S.A.* **91**, 9037 (1994).
- P. B. Rainey, M. Travisano, *Nature* **394**, 69 (1998).
- D. E. Rozen, R. E. Lenski, *Am. Nat.* **155**, 24 (2000).
- A. Buckling, P. B. Rainey, *Nature* **420**, 496 (2002).
- D. Schluter, *Am. Nat.* **157** (suppl.), S4 (2000).
- S. M. Vamori, D. Schluter, *Proc. R. Soc. London Ser. B* **269**, 923 (2002).
- R. F. Rosenzweig, R. R. Sharp, D. S. Treves, J. Adams, *Genetics* **137**, 903 (1994).
- R. Kassen, *J. Evol. Biol.* **15**, 173 (2002).
- S. Wright, *Genetics* **16**, 97 (1931).
- H. J. Muller, *Biol. Rev. Camb. Philos. Soc.* **14**, 261 (1939).
- A. Buckling, R. Kassen, G. Bell, P. B. Rainey, *Nature* **408**, 961 (2000).
- F. J. Ayala, C. A. Campbell, *Annu. Rev. Ecol. Syst.* **5**, 115 (1974).
- M. L. Rosenzweig, *Species Diversity in Space and Time* (Cambridge Univ. Press, Cambridge, 1995).
- P. B. Rainey, M. J. Bailey, *Mol. Microbiol.* **19**, 521 (1996).
- R. Kassen, A. Buckling, G. Bell, P. B. Rainey, *Nature* **406**, 508 (2000).
- Materials and methods are available as supporting material on Science Online.
- G. Bell, *Selection: The Mechanism of Evolution* (Chapman & Hall, London, 1997).
- A. R. Templeton, in *Epistasis and the Evolutionary Process*, J. B. Wolf, E. D. Brodie, M. J. Wade, Eds. (Oxford Univ. Press, Oxford, 2000).
- D. Schluter, *The Ecology of Adaptive Radiations* (Oxford Univ. Press, Oxford, 2000).
- We thank L. Hurst and three anonymous referees for comments on the manuscript. This work was funded by the Royal Society and Natural Environment Research Council (UK).

Supporting Online Material

www.sciencemag.org/cgi/content/full/302/5653/2107/DC1
Materials and Methods
References

7 July 2003; accepted 14 October 2003

Melt Inclusions in Veins: Linking Magmas and Porphyry Cu Deposits

Anthony C. Harris,^{1*} Vadim S. Kamenetsky,¹ Noel C. White,¹
Esmé van Achterbergh,² Chris G. Ryan²

At a porphyry copper-gold deposit in Bajo de la Alumbrera, Argentina, silicate-melt inclusions coexist with hypersaline liquid- and vapor-rich inclusions in the earliest magmatic-hydrothermal quartz veins. Copper concentrations of the hypersaline liquid and vapor inclusions reached maxima of 10.0 weight % (wt %) and 4.5 wt %, respectively. These unusually copper-rich inclusions are considered to be the most primitive ore fluid found thus far. Their preservation with coexisting melt allows for the direct quantification of important ore-forming processes, including determination of bulk partition coefficients of metals from magma into ore-forming magmatic volatile phases.

In porphyry ore deposits, metals are concentrated by large volumes of magmatic volatiles exsolved from crystallizing upper crustal magma bodies (1). Whether an ore deposit forms depends on the availability of metals in the magma, the partitioning of those metals into the volatile phase, and the history of the fluid after release from the magma (2–4). Ores are typically associated with hydrothermal mineral assemblages produced by the interaction of magmatic fluids with wall rocks (5). The earliest formed hydrothermal alteration of wall rocks is potassic (biotite-K-feldspar-quartz with or without magnetite assemblage) and is caused by high temperature (350° to 800°C) and saline (up to 70 weight % equivalent NaCl) fluids (6, 7). Discovery of silicate-melt inclusions coexisting with fluid inclusions in magmatic-hydrothermal quartz veins unambiguously links devolatilization of the magma with the associated porphyry ore deposit. This occurrence preserves the most primitive magmatic volatiles and the melt from which these were derived and, with the use of advanced microanalysis techniques, allows chemical changes to be traced through the evolution of the hydrothermal system. Moreover, we are able to use those data to quantify the magmatic-hydrothermal processes that lead to the formation of porphyry Cu deposits.

Bajo de la Alumbrera is an Au-rich porphyry Cu deposit where potassic alteration assemblages overprint several phases of porphyritic dacite intrusions and are associated with the bulk of the disseminated Cu-Fe sulfides and Au. High temperature (maximum of 750°C) and saline fluid (>35 wt % equivalent NaCl) of magmatic origin (as inferred from the calculated $\delta^{18}\text{O}$ and δD compositions) formed these alteration assemblages (8). Some of the earliest Cu-Fe sulfides occur in diffuse quartz veins, which are texturally similar to those described as A veins (9); however, the presence of silicate-melt inclusions warrants a new vein subclass. Hereafter we refer to them as P veins, reflecting their primitive role in the evolution of the magmatic-hydrothermal system. Typically, they consist of sugary quartz, with lesser amounts of K-feldspar and with or without hornblende-biotite-magnetite-chalcopyrite (CuFeS₂) and pyrite.

The P veins contain silicate-melt inclusions that consist of silicate crystals, vapor bubbles, salt crystals, and opaque oxide and sulfide crystals (Fig. 1). These inclusions are similar to those in magmatic quartz phenocrysts in the mineralized intrusions (10). Heating experiments (11) on silicate-melt inclusions revealed consistent phase transformations: The dissolution of the salt phases (e.g., halite and sylvite) occurs between 105° and 560°C; dissolution of crystalline silicate phases occurs between 650° and 765°C. After heating the host quartz crystals to 800°C at 1 atm external pressure for several hours, the sample was quenched to produce a silicate glass, which is extremely rich in K₂O compared to whole rock analyses and has a composition similar to K-feldspar (table S2). This composition may represent a chemically modified melt trapped in a dominantly aqueous environment or may contain ex-

¹Centre for Ore Deposit Research, University of Tasmania, Private Bag 79, Hobart, Tasmania 7001, Australia. ²Commonwealth Scientific and Industrial Research Organization Exploration and Mining, Post Office Box 136, North Ryde, New South Wales 1670, Australia.

*To whom correspondence should be addressed. E-mail: A.Harris@utas.edu.au

REPORTS

cess K-feldspar trapped with the evolved melt.

Remelted silicate-melt inclusions are not homogeneous but contain small (<1 to 8 μm) globules crowded with salt crystals, a vapor bubble (0.5 to 4 μm), and aqueous liquid (Fig. 2 and fig. S1). These inclusions represent the original entrapment of a two-phase system, i.e., melt and aqueous fluid. The inability to homogenize or remix the hypersaline fluid phase into the silicate melt, even after heating to high temperatures (up to 1000°C) or for extended periods (60 hours at 850°C), confirms that these silicate-melt inclusions represent heterogeneous trapping of phases immiscible at magmatic or near-magmatic conditions (12). Nondestructive in situ analysis by nuclear microprobe (proton-induced x-ray emission, or PIXE) was used to image the element distribution in heated silicate-melt inclusions (11). The data indicate that the highest concentrations of Cu and Fe reside in the Cl-rich fluid phase (Fig. 2 and fig. S2), consistent with the preferential partitioning of metals into the brine over the silicate melt from which these fluid phases were exsolved (13, 14).

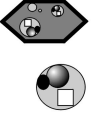


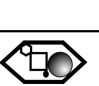
Fluid inclusions spatially associated with silicate-melt inclusions in the P veins at Bajo de la Alumbrera are divided into two groups: group 1, vapor-rich and polyphase hypersaline liquid-rich inclusions, and group 2, liquid-rich brine with few vapor-rich inclusions (Fig. 1). Fluid inclusions of group 1 coexist with silicate-melt inclusions in primary inclusion clusters interpreted to have been trapped during formation of the P veins. Group 2 inclusions occur in secondary trails that cut quartz and are related to later fracturing; therefore, these later inclusions preserve lower temperature and chemically evolved fluid.

Heating experiments (11) on primary group 1 hypersaline liquid inclusions revealed phase transformations that are similar to those observed in brine globules in the spatially and temporally associated silicate-melt inclusions. Final salt dissolution occurs between 480° and 540°C; complete homogenization of these fluid inclusions by vapor disappearance occurs from 745°C up to 845°C. The calculated salinities of the inclusions are up to 62 wt % equivalent NaCl, implying a magmatic origin, consistent with their temperature (7). No microthermometry

data could be obtained from the vapor-rich inclusions because of their small liquid content. PIXE analyses reveal that hypersaline liquid-rich inclusions can contain 10.0 wt % Cu (table S3). If analytical uncertainties of 20 to 30% are accounted for, the Cu concentration may vary by as much as 3.0 wt % (11). There is as much as 4.5 wt % Cu in coexisting vapor-rich inclusions. By contrast, the group 2 inclusions have lower homogenization temperatures ($\leq 550^\circ\text{C}$) and salinities up to 58 wt % equivalent NaCl. These brine inclusions have Cu concentrations below 1.0 wt %, as determined by laser ablation inductively coupled plasma mass spectrometry (8) and our PIXE analyses. However, not all aqueous fluids associated with P veins contain very high Cu concentrations. A high-temperature polyphase hypersaline liquid-rich inclusion from a P vein in a different intrusion with lower Cu grades contained about 0.5 weight % Cu (11) (table S3).

Unusually high Cu concentrations in fluids trapped in some group 1 inclusions are consistent with these being the most primitive magmatic-hydrothermal fluids found at Bajo de la Alumbrera. The high Cu concentrations in the fluid dropped during the earliest stages of mineralization (Fig. 3). Fe/Zn parallels the Fe/Pb ratio, whereas Fe/Cu rises, indicating the removal of Cu from the fluid. Our results suggest that the absolute Zn and Pb concentrations in the group 2 inclusions are slightly higher than those in the group 1 inclusions. Because PIXE analysis of Cl is sensitive to the thickness of quartz above the inclusion, Br is used as a proxy for Cl. The Zn/Br and Pb/Br (and by inference, Cl) ratios remain constant (Fig. 3), suggesting that the slight enrichment of Zn and Pb probably resulted from separation of the low-salinity vapor from the hypersaline portion of the ore fluid. Appreciable Cu concentrations in vapor-rich group 1 fluid inclusions imply the formation of volatile Cu complexes, as found in studies of other porphyry Cu and Sn-W systems (8, 15, 16).

PIXE analyses of vapor and brine inclusions coexisting with homogenized silicate melt inclusions (fig. S2 and table S3) have been used to determine a preliminary brine/vapor partition coefficient for Cu of $D_{\text{Cu, brine/vapor}} = 1.5$ to 2.

Type & Description	
	Silicate-melt inclusions with brine globules: Silicate crystals - vapor (20-40 volume %) \pm salt(s)-chalcopyrite - magnetite. Size varies between 5 and 25 μm , up to 45 μm . Occur as negative crystals or are spherical. Minor amounts of liquid associated with halite (?sylvite) crystals.
	Vapor-rich fluid inclusions: Vapor - chalcopyrite \pm liquid (<10 volume %). Elongate ellipsoidal inclusions or negative crystal shapes (5-35 μm).
	Polyphase hypersaline fluid inclusions: Salts (halite-sylvite) - anhydrite - vapor - liquid \pm chalcopyrite - magnetite (hematite). Biotite, hornblende, apatite, and rutile also occur. There are several other as yet unidentified opaque phases. Elongate ellipsoidal inclusions or negative crystal shapes (5-40 μm).
	Brine fluid inclusions: Halite - liquid - vapor (<20 volume %) \pm chalcopyrite. Negative crystal shapes (<35 μm).

Inclusion association and distribution

Quartz Phenocrysts

Magmatic Inclusions



P veins

GROUP 1: Primary inclusions

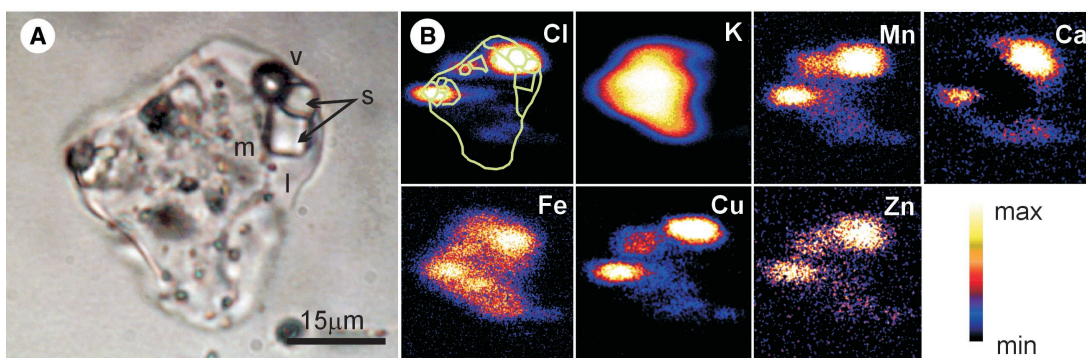


GROUP 2: Secondary inclusions



Fig. 1. Definition of inclusion populations observed in quartz from porphyritic intrusions at Bajo de la Alumbrera [modified after Ulrich *et al.* (8)]. Silicate-melt (gray hexagon) and aqueous (white hexagon) inclusion symbols are filled with vapor bubbles (shaded circles), salt crystals (open squares and polygons), and opaque oxide and sulfide crystals (black shapes).

Fig. 2. Partly homogenized volatile-rich silicate-melt inclusion in a sulfide-bearing P vein. (A) Optical image; besides a silicate melt portion (m), this inclusion has multiple salt phases (s) and vapor bubbles (v). (B) PIXE element distribution maps (11). Legend shown in lower right corner indicates increasing intensity (and thus concentration). Color scale for each image is normalized to its own maximum. The inclusion outline is laid over the Cl map.



The extremely high Cu contents found in group 1 inclusions indicate that the brine/melt partition coefficient under the prevailing conditions (temperature, pressure, oxygen fugacity, and salinity) must have been very high unless unreasonably high Cu concentrations in the magma are assumed. For Cu_{melt} of 50 to 200 parts per million (ppm), $D_{Cu, brine/melt}$ equals 500 to 2000.

On the basis of the calculated salinity and measured temperature of fluid inclusions, combined with experimental data on the NaCl-H₂O system, we can estimate the minimum pressure of formation (17). Fluid-inclusion assemblages (comprising coexisting low-density vapor and hypersaline fluid) trapped in the bulk of the hydrothermal alteration at Bajo de la Alumbrera have pressures of ~30 MPa (8); however, pressures as high as 100 MPa (equivalent to ~4 km depth under lithostatic pressure) have been determined for inclusion assemblages in the P veins (fig. S3). The contrasting pressure conditions are explained by the early exsolution of group 1 fluids from the magma while the confining carapace was still intact and confining pressure was at a maximum. Subsequent volatile exsolution occurred from the magma after rupturing of the carapace and shattering of the overlying rock column.

Our data from Bajo de la Alumbrera show that the earliest aqueous volatile phase to exsolve from the magma (group 1) separated into two aqueous phases, one comprising

about 20 volume % (an approximation based on the modal abundance of fluid inclusions) of brine containing ~53 weight % equivalent NaCl and 10% Cu, the other comprising about 80 volume % of vapor containing ~2.0 wt % equivalent NaCl and ~4.5% Cu. Numerical models anticipated similar phase proportions, salinities, and metal concentrations from the unmixing of an originally homogeneous aqueous fluid (with salinity ~8.5 wt % equivalent NaCl) exsolved from a subjacent magma at ~100 MPa (18). Furthermore, the observed Cu concentrations are as high or higher than those previously reported from other inclusion studies (8, 14) and experimental modeling of crystallizing melts (3, 18).

We infer that decompression from 100 MPa to ~30 MPa and cooling from >745° to <550°C caused evolution of exsolved fluids (group 1 to group 2) and deposition of Cu in the earliest evolution of this porphyry ore deposit. Evidence for this comes in part from the PIXE data that reveal between 5 and 10 times higher levels of Cu occur in some early high-temperature and pressure aqueous phases (group 1) than in the moderate temperature brines (group 2). The data also show near-constant Zn/Pb, Zn/Br, and Pb/Br (and by inference, metal/Cl) ratios, from one stage to the next, implying that the earliest fluid (group 1) evolved to the second (group 2). To do that, the evolving magmatic fluid lost a substantial amount of Cu (up to 10 wt % Cu to

below 1 wt % Cu; also implicit in the observed Fe/Cu ratios), which was deposited from the pristine magmatic fluids during or after rupturing of the rock column. Decompression would produce further phase separation of the early-formed magmatic volatile phases, producing new low-density aqueous vapor phases and hypersaline liquids. This aqueous phase immiscibility probably caused additional deposition of Cu-Fe sulfides. Halite may also have precipitated (8). Once in a predominantly hydrostatic regime, any change in temperature, pH, and/or oxygen fugacity of the system would have caused Cu-Fe sulfides to deposit from the exsolved magmatic fluid (8, 19).

References and Notes

1. J. W. Hedenquist, J. B. Lowenstern, *Nature* **370**, 519 (1994).
2. J. B. Lowenstern, G. A. Mahood, M. L. Rivers, S. R. Sutton, *Science* **252**, 1405 (1991).
3. P. A. Candela, P. M. Piccoli, in *Magmas, Fluids, and Ore Deposits*, vol. 23 of *Short Course Series*, J. F. H. Thompson, Ed. (Mineralogical Association of Canada, Ottawa, Canada, 1995), pp. 101–127.
4. T. J. Williams, P. A. Candela, P. M. Piccoli, *Contrib. Mineral. Petrol.* **121**, 388 (1995).
5. J. J. Hemley, J. P. Hunt, *Econ. Geol.* **87**, 23 (1992).
6. R. E. Beane, S. R. Titley, *75th Anniv. Vol. Econ. Geol.* p. 235 (1981).
7. R. J. Bodnar, in *Magmas, Fluids, and Ore Deposits*, vol. 23 of *Short Course Series*, J. F. H. Thompson, Ed. (Mineralogical Association of Canada, Ottawa, Canada, 1995), pp. 139–152.
8. T. Ulrich, D. Günthür, C. A. Heinrich, *Econ. Geol.* **97**, 1889 (2002).
9. L. B. Gustafson, J. P. Hunt, *Econ. Geol.* **70**, 857 (1975).
10. A. C. Harris, V. S. Kamenetsky, N. C. White, in *Mineral Exploitation and Sustainable Development: Proceedings of the Seventh Biennial Meeting, Society for Geology Applied to Mineral Deposits*, D. G. Eliopoulos et al., Eds. (Millpress, Rotterdam, Netherlands), pp. 275–278.
11. Materials and methods are available as supporting material on Science Online.
12. V. S. Kamenetsky et al., in *Melt Inclusions in Volcanic Systems Methods, Applications and Problems*, vol. 5 of *Developments in Volcanology*, E. De Vivo, R. Bodnar, Eds. (Elsevier, Amsterdam, 2003), pp. 65–85.
13. P. Davidson, V. S. Kamenetsky, *Econ. Geol.* **96**, 1921 (2001).
14. V. S. Kamenetsky et al., *Chem. Geol.* in press.
15. C. A. Heinrich et al., *Econ. Geol.* **87**, 1566 (1992).
16. C. A. Heinrich et al., *Geology* **27**, 755 (1999).
17. R. J. Bodnar et al., *Geochim. Cosmochim. Acta* **49**, 1861 (1985).
18. C. W. Burnham, in *Geochemistry of Hydrothermal Ore Deposits*, H. L. Barnes, Ed. (Wiley, New York, ed. 3, 1997), pp. 63–123.
19. A. Hezarkhani, A. E. Williams-Jones, *Econ. Geol.* **93**, 651 (1998).
20. The Centre for Ore Deposit Research directly funded this work. Samples used in this study were collected during A.C.H.'s research at the University of Queensland, funded by MIM Exploration. We thank D. Steele for valuable assistance with microprobe analyses and D. Cooke, J. Hedenquist, M. Solomon, and three anonymous referees for detailed and helpful reviews of this manuscript.

Supporting Online Material

www.sciencemag.org/cgi/content/full/302/5653/2109/DC1
Materials and Methods
Figs. S1 to S3
Tables S1 to S3

31 July 2003; accepted 7 November 2003

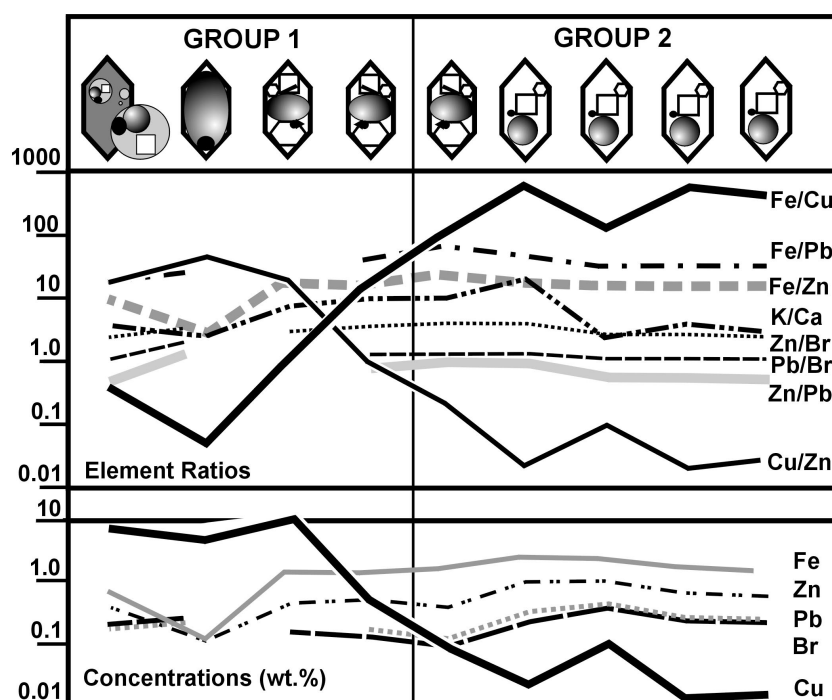


Fig. 3. Element ratios and concentrations from representative liquid compositions from silicate-melt and fluid inclusions from Bajo de la Alumbrera (table S3). The temporal evolution of the system is broadly from left (group 1, primary inclusions) to right (group 2, secondary inclusions). The analyzed silicate-melt inclusion was heated to reveal a single brine globule.

Supporting Online Material

Material and methods

Vein material for inclusion analysis was sampled from drillcore and mine workings at the Bajo de la Alumbrera porphyry Cu-Au deposit. Representative samples from the earliest alteration stages were selected for analysis. Temporal variations in silicate-melt and fluid inclusions were identified with detailed petrographic observations. Inclusion populations were studied using doubly polished thick sections. Homogenization experiments on silicate-melt and fluid inclusions were performed at 1-atm using a high temperature LINKAM TS1500 heating stage. At high temperatures, the uncertainty in the observed temperature is less than 20°C. Salinity was calculated from the dissolution temperature of halite and assumes a simple NaCl-H₂O system (*S1*). All temperatures are uncorrected for pressure, and therefore lower than the true trapping temperature.

Non-destructive in situ nuclear microscopy by PIXE (**P**roton **I**nduced **X**-ray **E**mission) was used to image the element distribution of remelted silicate-melt inclusions. PIXE technology uses a high-energy proton beam (3 MeV) focused to 1.3 µm diameter to penetrate quartz, exciting X- and γ-rays from elements in subsurface silicate-melt or fluid inclusions (*S2*, *S3*). Samples were prepared as doubly polished thick sections. Inclusions were prepared to within ~10 µm of the surface, then photographed and measured (including size and depth) prior to the sample being carbon coated. Element concentration maps were produced by raster scanning the inclusions. Using the Dynamic Analysis method (*S2*), element concentrations are calculated accounting for the inclusion geometry, depth of the inclusion below the surface and an estimated fluid density. Dynamic Analysis is a standardless technique that calculates element concentration from first principles (*S4*, *S5*) and corrects for detector solid angle and matrix effects. Individual inclusions were analyzed for up to 20 minutes. A 250 µm Be filter was placed in front of the Si(Li) X-ray detector to

reduce the intensity of the background signal. Analytical uncertainty of this technique is estimated at 20-30%, with higher uncertainty for elements lighter than potassium.

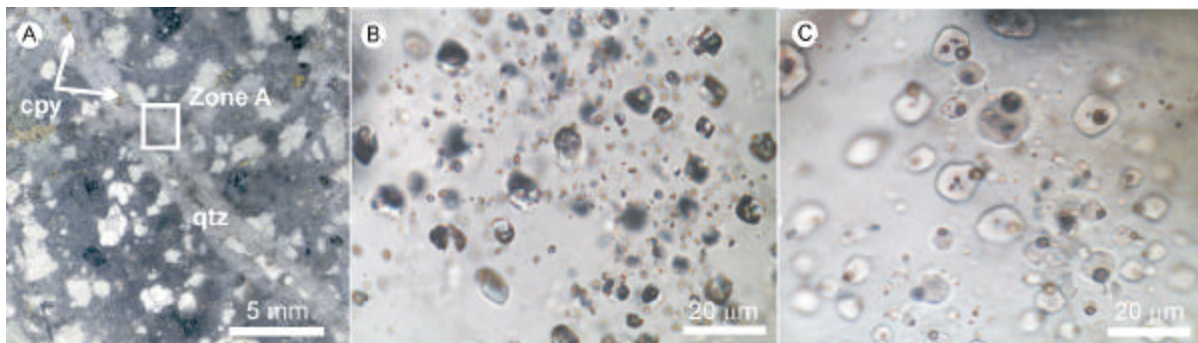


Figure S1. Silicate-melt inclusions in mineralised quartz veins. **A.)** P vein that cross cuts potassically-altered dacite at Bajo de la Alumbreira. Chalcopyrite (cpy) is intergrown with vein quartz (qtz). Small intergrowths of K-feldspar, biotite, and hornblende also fill the vein core. The vein margins are ragged and diffuse. **B.)** Transmitted light photomicrograph of a cluster of silicate-melt inclusions (zone A in previous photo). These darkish grey silicate-melt inclusions are visibly different to brine-rich fluid inclusions typically reported in potassic alteration (8). **C.)** When heated and quenched after 26 hours at 850°C the aluminosilicate content homogenizes to reveal small globules of salt phases with contrasting relief compared to the silicate melt.

Table S1. Rock sample location and description

Sample	Location	Description
99102	Diamond Drill Hole 48.4-54 124.4 metres	Early P3 Porphyry with relatively pristine magmatic biotite and plagioclase phenocrysts. Round quartz eyes abundant. Ragged hornblende phenocrysts also occur. Trace apatite and zircon. Quartz-feldspar groundmass is altered by biotite \pm ?illite – this alteration in part alters some plagioclase phenocrysts. P veins consist of quartz, with lesser amounts of K-feldspar \pm hornblende-biotite-magnetite-chalcopyrite and pyrite. Veinlets of magnetite also occur, as does chlorite \pm ?illite veins.
99166	Diamond Drill Hole 48.5-54 139 metres	P2 Porphyry consisting of plagioclase and rare biotite and quartz. Intense ?illite alteration of plagioclase. Biotite altered by chlorite. Stockwork of veinlets of quartz-chalcopyrite \pm biotite-K-feldspar. Stringers of chalcopyrite very abundant. Rare diffuse P quartz veins.
0301	Mine Bench ~2450 m ASL -66°36'30.708 -27°19'41.88	Biotite-magnetite-quartz \pm K-feldspar altered ?P2 Porphyry. Intense pervasive biotite-magnetite alteration obscures phenocrysts and groundmass. Biotite phenocrysts are recrystallized and the groundmass feldspars are altered to a mosaic of biotite-quartz-K-feldspar \pm chlorite-rutile-apatite. P quartz veins cut this pervasive alteration. The veins are diffuse with sugary quartz. Chalcopyrite and lesser K-feldspar are intergrown with the quartz. Chlorite \pm illite alteration affects the biotite phenocrysts and less commonly the secondary biotite.

Table S2. Whole rock geochemistry of mineralized porphyries compared to microprobe chemistry of silicate-melt inclusions found in quartz veins in overprinting hydrothermal alteration.

	Early P3*	Late P3*	Late Porphyry*	Silicate-melt inclusion in quartz phenocryst †		Silicate-melt inclusion in quartz vein †		Silicate-melt inclusion in quartz vein †	
Sample ID	43-47.1/580	BLA 48	BLA 44	99102_4 ‡		99166_13		99166_35	
Analyses				n = 4		n = 4		n = 3	
SiO ₂ wt. %	65.9	65.61	64.2	66.86	± 1.01	65.91	± 0.40	67.41	± 2.10
TiO ₂	0.56	0.64	0.66	<0.04		<0.01		<0.07	
Al ₂ O ₃	15.80	16.00	15.50	16.19	± 0.05	18.48	± 0.45	17.73	± 1.13
FeO	2.2	4.92	2.5	0.41	± 0.35	0.06	± 0.05	<1.08	
MnO	0.1	0.11	0.1	<0.03		<0.01		<0.01	
MgO	1.5	1.78	1.7	<0.01		<0.01		<0.01	
CaO	3.4	3.99	2.6	<0.03		0.07	± 0.02	0.06	± 0.05
Na ₂ O	3.2	2.44	3.3	2.00	± 0.17	2.31	± 0.16	2.64	± 0.15
K ₂ O	4.05	3.62	3.98	11.92	± 2.42	13.44	± 0.37	12.42	± 0.53
P ₂ O ₅	0.3	0.11	0.3	<0.01		<0.02		<0.08	

* Whole rock analyses published by Ulrich and Heinrich (S6)

† Melt inclusion chemistry determined using a Camica SX-50 at the University of Tasmania. Analyses were performed using an accelerating voltage of 15 kV and a 25 nA beam current

‡ Sample ID is the Sample number (Table S1) plus an inclusion identifier

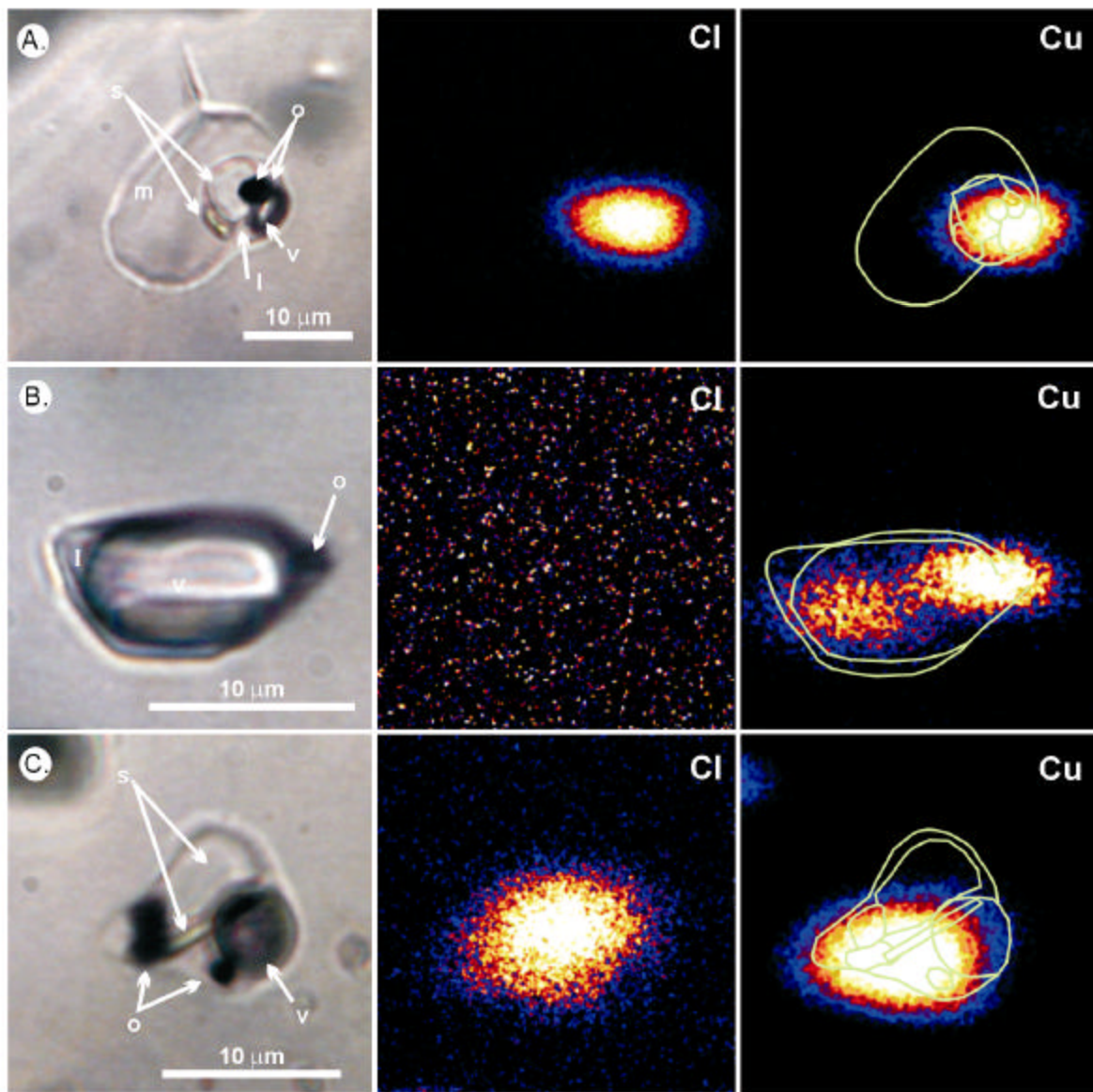


Figure S2. PIXE element distribution maps of primary silicate-melt and fluid inclusions in P veins. **A.)** Volatile-rich silicate-melt inclusion in sulfide-bearing P vein. The original small silicic aggregates homogenized (m) when heated to 850°C for 26 hours. Upon quenching a salt-bearing globule formed. Beside salts (s; one of which is halite), there are numerous opaque phases (o), a vapor bubble (v) and a small liquid component (l). To the right of the photomicrograph are the PIXE element distribution maps for Cl and Cu, respectively. Legend and color scale is the same for *Fig 1*. The inclusion outline is laid over the Cu map. **B.)** Vapor-rich fluid inclusion coexisting with silicate-melt inclusions in P

vein. Besides a distinct vapor bubble (v) there is a small liquid component (l) and an opaque phase (o). C.) Polyphase hypersaline liquid-rich inclusion that coexists with silicate-melt inclusions in a P vein. Besides a liquid component, there is a distinct vapor bubble (v). Moreover, this inclusion is crowded with numerous opaque phases (o) and salts (s), possibly including sulfates.

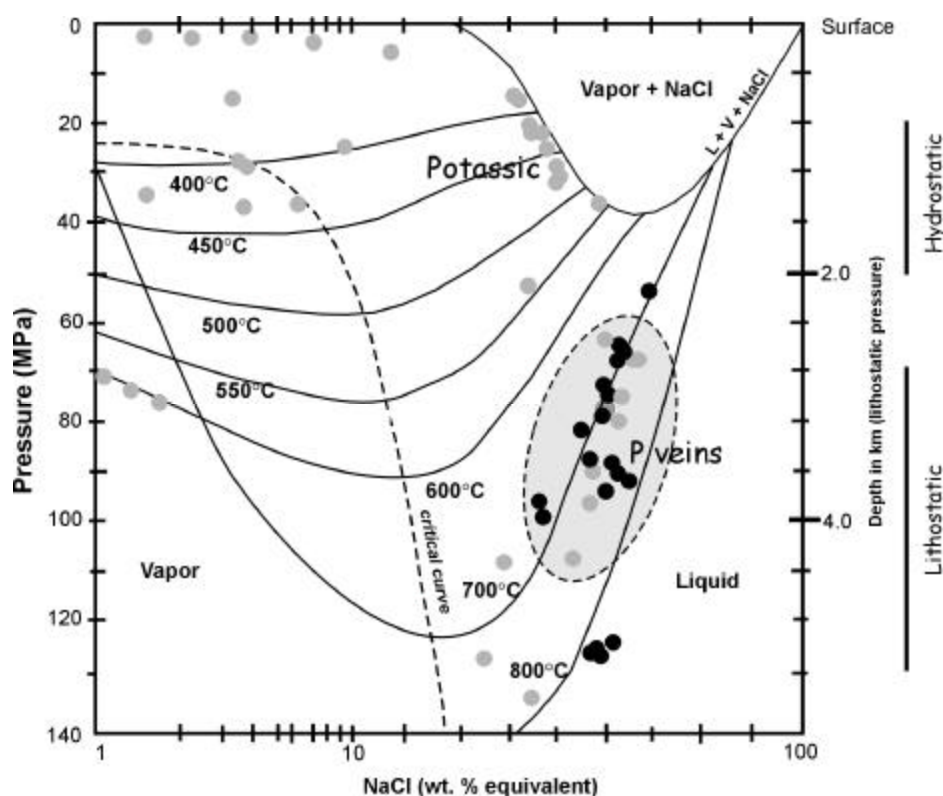


Figure S3. Pressure-NaCl phase diagram contoured with temperature (modified after Ulrich et al. and references therein; 8). Grey circles represent the data of Ulrich et al. (8). Black circles are aqueous phase equilibria from this study. Primary inclusions found in P veins have a higher pressure than those in the bulk of the potassic alteration assemblages (8). Independent geologic evidence exists to show that at the time of mineralization the total thickness of rock above the magmatic-hydrothermal system was ≥ 2.5 km (S7) – these depths would correspond to lithostatic pressures between 70 and 100 MPa. Note that coexisting with some of our primary P vein hypersaline inclusions are vapor-rich inclusions

of indeterminate salinity. Based on available aqueous phase equilibria these vapor-rich inclusions should have salinity < 5.0 wt.% equivalent NaCl (17).

Supporting references

- S1. R. J. Bodnar, M. O. Vityk, IMA short course volume (Virginia Polytechnic Institute State Univ. Press, 1994), pp. 117-130.
- S2. C. G. Ryan *et al.*, *Nucl. Instrum. Methods*. **B104**, 157 (1995).
- S3. C. G. Ryan *et al.*, *Nucl. Instrum. Methods*. **B181**, 570 (2001).
- S4. C. G. Ryan *et al.*, *Nucl. Instrum. Methods*. **B77**, 463 (1993).
- S5. C. G. Ryan *et al.*, *Nucl. Instrum. Methods*. **B158**, 18 (1999).
- S6. T. Ulrich, C. A. Heinrich, *Econ. Geol.* **97**, 1865 (2002).
- S7. A. C. Harris *et al.*, *Mineralium Deposita*, in press (DOI: 10.1007/s00126-003-0381-0).



Table S3. Element concentration data for fluid inclusions from Bajo de la Alumbrera, analyzed by PIXE.

	Magmatic Inclusions		Group 1*			Group 1	Group 2				
Inclusion Type											
Size X (length)	17.0	10.0	6.5	12.8	9.3	25.0	18.0	20.6	15.3	17.8	15.8
Size Y (width)	12.0	12.0	8.0	7.6	8.2	11.0	9.0	16.9	10.0	12.5	9.4
Size Z (Thickness)	12.0	7.5	7.0	3.0	5.0	11.5	6.5	9.5	4.5	9.0	9.0
Midplane	18.0	13.5	6.0	15.0	7.5	12.0	25.5	13.5	12.0	10.5	16.5
Depth	12.0	9.8	2.5	13.5	5.0	6.3	22.3	8.8	9.8	6.0	12.0
Assumed density	2.0	1.2	1.2	0.5	1.2	1.2	1.2	1.2	1.2	1.2	1.2
Sample ID	99102_4	99102_5	0301_1	0301_2	0301_3	99166_14	99166_15	99166_17	99166_19	99166_20	99166_21
Cl (ppm)	DEEP †	152950	249410	DEEP	67520	74020	DEEP	272030	282100	215560	DEEP
K	9800	41040	N.D.	12550	26500	25710	58110	91020	67570	63340	29590
Ca	1200	5770	8120	4420	3530	2580	5720	4490	28690	16370	9870
Ti‡	550	1380	BDL	2440	440	700	10780	1300	1510	550	730
Mn	3400	11580	8180	360	11510	10650	10220	22190	31600	21990	16850
Fe	8900	83630	31040	2270	76700	76260	89600	159670	148150	94430	83360
Cu	1300	2310	73570	49430	95680	5280	930	240	1050	150	170
Zn	1200	4700	3780	1060	4800	5160	4050	10130	10430	6820	5900
Ge	BDL §	BDL	BDL	930	BDL	BDL	100	BDL	150	BDL	BDL
As	BDL	BDL	170	BDL	140	BDL	BDL	BDL	BDL	BDL	BDL
Br	330	1720	1660	BDL	1570	1400	980	2480	3890	2560	2330
Rb	BDL	530	BDL	BDL	370	400	520	750	1030	910	850
Sr	180	290	BDL	BDL	BDL	190	BDL	250	710	540	420
Ba	770	BDL	BDL	BDL	1360	BDL	BDL	BDL	BDL	BDL	BDL
Pb	240	1740	1600	BDL	BDL	1850	1300	3290	4410	2890	2680

* Coexisting inclusions used to calculate brine/melt and brine/vapor partition coefficients of Cu. The melt composition is estimated from typical melt compositions, whereas the brine and vapor components are directly measured. Inclusion 0301_1 is a brine globule in a composite silicate-melt inclusion.

† DEEP denotes those inclusions that were too deeply buried beneath the sample surface for Cl to be quantified

‡ Ti is not likely to be in inclusions, rather it is probably dispersed as rutile inclusions through the quartz host

§ BDL = below detection limit